Microarray Analysis of Differential Gene Expression Between Traumatic Temporomandibular Joint Fibrous and Bony Ankylosis in a Sheep Model

Authors' Contribution:
Study Design A
Data Collection B
Statistical Analysis C
Data Interpretation D
Manuscript Preparation E
Literature Search F
Funds Collection G

BCDEF 1 **Tong-Mei Zhang***
BCD 2 **Kun Yang***
AB 3 **Su-Xia Liang**
AB 4 **Pei-Pei Zhang**
BD 1 **Hua-Lun Wang**
CD 1 **Yuan-Yuan Tian**
BC 1 **Zhao-Yuan Xu**
ABCDG 1 **Hao Liu**
ABCDEFG 1 **Ying-Bin Yan**

1 Department of Oromaxillofacial – Head and Neck Surgery, Tianjin Stomatological Hospital, Tianjin, PR China
2 Tianjin Medical University, Tianjin, PR China
3 Department of Operative Dentistry and Endodontics, Tianjin Stomatological Hospital, Tianjin, PR China
4 Department of Stomatology, Xuzhou Central Hospital, Xuzhou, Jiangsu, PR China

Corresponding Authors:
Financial support:

* Tong-Mei Zhang and Kun Yang contributed equally to this paper
Hao Liu, e-mail: kqlh2013@163.com, Ying-Bin Yan, e-mail: yingbinyan@qq.com
This investigation was supported by Tianjin Key Discipline Foundation of Clinical Medicine (HWZX001 and HWZX003) and the State Key Laboratory of Medicinal Chemical Biology (Nankai University) (2010022)

Background: The type of traumatic temporomandibular joint (TMJ) ankylosis depends on the degree of severity of TMJ trauma. Here, we performed comprehensive differential molecular profiling between TMJ fibrous and bony ankylosis.

Material/Methods: Six sheep were used and a bilateral different degree of TMJ trauma was performed to induce fibrous ankylosis in one side and bony ankylosis in the other side. The ankylosed calluses were harvested at days 14 and 28 postoperatively and analyzed by Affymetrix OviGene-1_0-ST microarrays. DAVID was used to perform the Gene Ontology and Kyoto Encyclopedia of Genes and Genomes pathway analysis for the different expression genes (DEGs). The DEGs were also typed into protein–protein interaction (PPI) networks to get the interaction data. Ten DEGs, including 7 hub genes from PPI analysis, were confirmed by real-time PCR.

Results: We found 90 and 323 DEGs at least 2-fold at days 14 and 28, respectively. At day 14, bony ankylosis showed upregulated DEGs, such as TLR8, SYK, NFKBIA, PTPRC, CD86, ITGAM, and ITGAL, indicating a stronger immune and inflammatory response and cell adhesion, while genes associated with anti-adhesion (PRG4) and inhibition of osteoblast differentiation (SFRP1) had higher expression in fibrous ankylosis. At day 28, bony ankylosis showed increased biological process related to new bone formation, while fibrous ankylosis was characterized by a prolonged immune and inflammatory reaction.

Conclusions: This study provides a differential gene expression profile between TMJ fibrous and bony ankylosis. Further study of these key genes may provide new ideas for future treatment of TMJ bony ankylosis.

Keywords: Microarray Analysis • Models, Animal • Sheep • Temporomandibular Ankylosis • Temporomandibular Joint

Full-text PDF: https://www.medscimonit.com/abstract/index/idArt/932545

📄 5549   📊 2   📈 10   📑 64

Background

Temporomandibular joint (TMJ) ankylosis is a severely disabling disease characterized by a progressive limitation of mouth opening due to craniomandibular fusion [1,2]. Trauma is the leading cause of the condition, and other causes include local or systemic infection, ankylosing spondylitis, and rheumatoid arthritis [3,4]. Although better and earlier management of condylar fractures and modern antibiotic treatment have reduced the incidence, it is still not uncommon in developing countries [3,5].

TMJ ankylosis can be classified into fibrous, fibro-osseous, or bony, according to the tissue involved [3], in which bony ankylosis accounts for the vast majority of cases [2,4,6-8]. Bony ankylosis is a more challenging problem than fibrous ankylosis because of the technical difficulties and the high incidence of recurrence [5,9]. Recent clinical and experimental studies showed that traumatic TMJ bony ankylosis might evolve from not fibrous ankylosis, but rather from fibro-osseous ankylosis [8,10-12], which indicates that fibrous and bony ankylosis might be the result of 2 different pathological processes. Although the specific traumatic microenvironment for the development of ankylosis is still unclear, our previous animal studies demonstrated that once the physical barriers (the disc and the fibrous layers covering on the condyle and the glenoid fossa) were damaged, ankylosis inevitably occurred [13,14]. In these cases, the types of ankylosis depended on the degree of severity of TMJ trauma, with severe trauma corresponding to bony ankylosis and minor trauma corresponding to fibrous ankylosis [10,11].

Since patients with fibrous ankylosis have milder clinical presentations and better prognosis than those with bony ankylosis, a conversion of bony ankylosis into fibrous ankylosis might be a new strategy for blocking the progression or even the onset of bony ankylosis, which largely depends on advanced understanding of the molecular mechanisms underlying the association between the TMJ traumatic microenvironment and the types of ankylosis. Based on a reliable sheep model, our previous studies demonstrated that fibrous ankylosis was related to reduced angiogenesis [10] and a lack of key growth factors regulating osteogenesis and chondrogenesis [15,16] in comparison to bony ankylosis, which indicated that some significant biological pathways were involved in determining the types of ankylosis after TMJ trauma. However, these studies only examined a small number of interesting genes. A comprehensive differential molecular profiling regarding the 2 types of ankylosis is needed.

Microarray analysis is a powerful technique which enables researchers to detect the relative concentration of tens of thousands of transcripts in a single experiment, thereby becoming a common approach for screening novel candidate genes relating to a certain physiopathology, for example, TMJ osteoarthritis [17]. Recently, researchers have used this method to explore gene expression pattern during the healing of condylar fracture in a lateral pterygoid muscle preserved group versus a lateral pterygoid muscle resection group [18], which shed light on the role of lateral pterygoid muscle in the formation of TMJ ankylosis. However, the type of ankylosis was not specified in the experiment [18]. A comprehensive study of the differential gene expression profiles between fibrous and bony ankylosis is needed.

According to the pathological examination of our animal model, days 14 and 28 were the 2 critical time-points to differentiate bony ankylosis from fibrous ankylosis [10,11]. At day 14, no cartilage formed in both types of ankylosed joint; however, coarse collagen and remnants of the hematoma could be found in the fibrous but not bony ankylosed joints, indicating prolonged presence of hematoma during the development of fibrous ankylosis [10,11]. At day 28, endochondral ossification occurred in the bony ankylosis, while fibrous tissue occupied the joint space without cartilage formation in the fibrous ankylosis [10,11]. Therefore, the differential molecular profilings at the 2 key time-points would help clarify the molecular mechanisms determining the types of traumatic TMJ ankylosis.

In the present study, high-throughput Affymetrix® OviGene-1_0-ST microarrays were employed to simultaneously compare the gene expression of over 22 047 transcripts between the TMJ fibrous and bony ankylotic callus harvested at days 14 and 28 postoperatively, using a reliable sheep model. We aimed to discovery some novel candidate genes or signal molecules which were specifically linked to TMJ fibrous or bony ankylosis based on the comprehensive differential molecular profiling. These findings may provide new insights into the therapeutic or preventive methods for TMJ ankylosis in the future.

Material and Methods

Animal Model and Tissue Harvest

This study was approved by the Ethics Committee of the Tianjin Stemmatological Hospital (Tjskq2013001). Six local-strain male Xiaowei-Han sheep (3 months old, with preoperative weight ranging from 18 to 22 kg) were used in the study. The housing and husbandry conditions, including bedding material, breeding program, light/dark cycle, temperature, quality of water, and type of food were the same as previously described [14]. The traumatic TMJ ankylosis model was established according to the protocol outlined in previous publications [10,11]. General anesthesia was induced by intravenous injection of 10 mg/kg pentobarbital sodium with tracheal intubation, and the
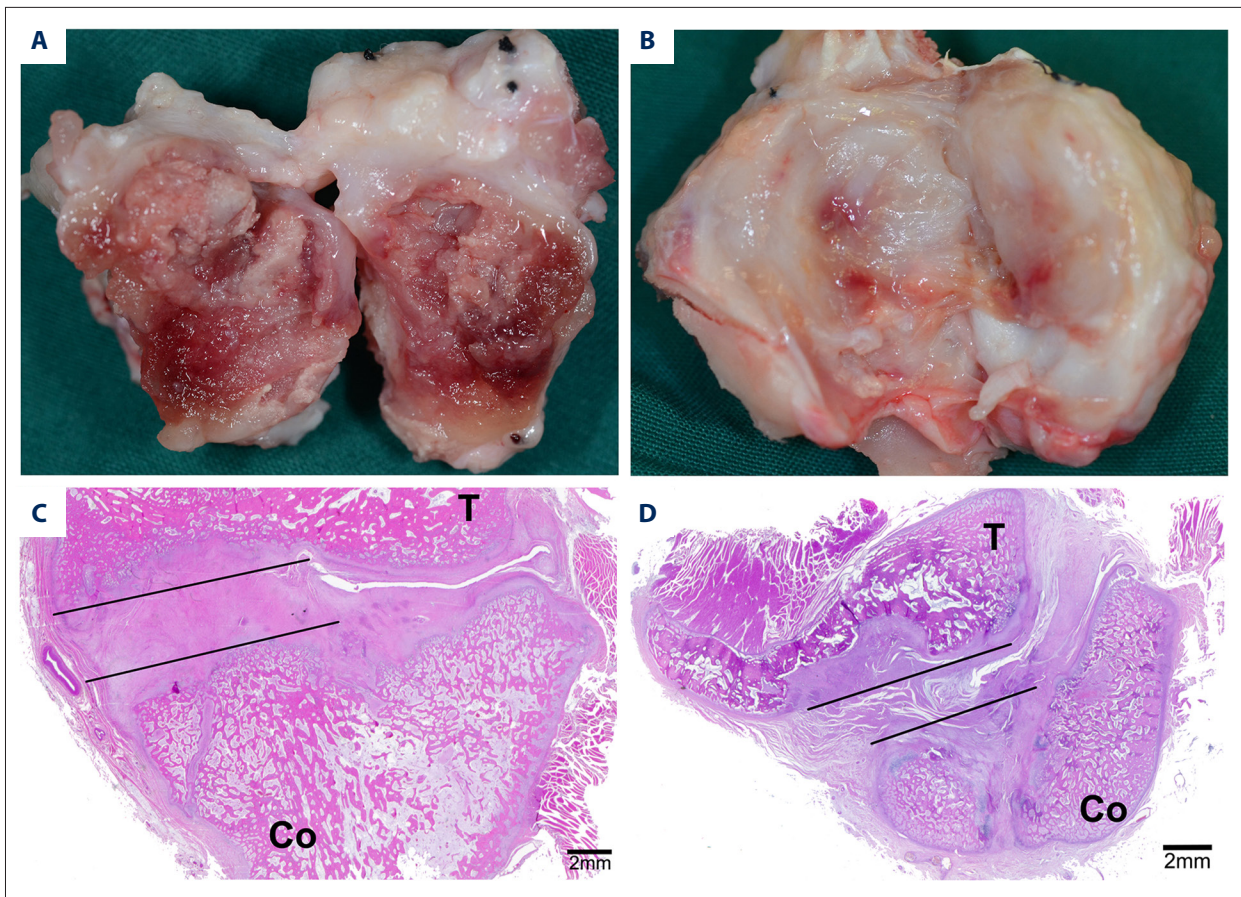
Figure 1. The site of tissue harvesting. (**A**) The ankylosed joint was split open at day 14. (**B**) The ankylosed joint was split open at day 28. (**C**) The area marked by the lines showed the bony ankylosed callus. (**D**) The area marked by the lines showed the fibrous ankylosed callus. T – temporal bone; Co – condyle.

anesthetic time could be extended by intravenous injection of 5 mg/kg/h propofol when necessary. To relieve pain in animals, carprofen was intravenously administered at 3 mg/kg before surgery, and local-infiltration anesthesia was performed along the incision with lidocaine (4 mg/kg). All animals received bilateral condylar sagittal fracture and discectomy. On one side of the TMJ, animals received an additional severe damage to the glenoid fossa, namely carving deep grooves in the glenoid fossa until the exposure of cancellous bone with bleeding, which had been previously shown to support bony ankylosis [10,11]. On the contralateral TMJ, animals received additional minor damage to the glenoid fossa, namely removal of the fibrous layer covering on the glenoid fossa, thereby producing a distinctly fibrous ankylosis [10].

Carprofen (4 mg/kg) was given intravenously every 24 h for 3 days postoperatively to relieve pain. Three animals were sacrificed through euthanasia with a lethal dose of pentobarbitone sodium (120 mg/kg) through the external jugular vein at days 14 and 28 after surgery, respectively. Animal death was verified by observing the cessation of breathing and heartbeat,

and the disappearance of pupillary light reflex and nerve reflex. The bilateral TMJ complexes were removed en bloc with a band saw. Then, any soft tissue was promptly dissected from around the joint. The ankylosed joints were split open carefully using a narrow osteotome, and the newly generated tissues in the joint space, namely fibrous or bony ankylosed callus (**Figure 1**), were harvested as previously described [15]. The ankylosed callus with the total volume of about 0.5-1.0 mL for each sample was rapidly frozen in liquid nitrogen and stored at -80°C for ribonucleic acid (RNA) extraction.

RNA Preparation and Microarray Data Acquisition

For each of the 3 samples per time-point, the RNA preparation and microarray assay were performed by the CNKINGBIO Corporation (Beijing, China). In brief, total RNA was extracted from ankylosed callus using TRIzol reagent (Invitrogen Life Technologies, Carlsbad, USA) and purified with an RNeasy mini kit (Qiagen, Valencia, USA) per the manufacturer's protocol. When we isolated RNA from each sample, one part of ankylosed callus with the size of about 100 μL was used, and 1 mL

of TRIzol reagent was added. Then, biotinylated complementary deoxyribonucleic acid (cDNA) was prepared according to the standard Affymetrix protocol from 150 ng total RNA using the Ambion® WT Expression Kit. After labeling, fragmented cDNA was hybridized for 16 h at 45°C on the Gene Chip Affymetrix® OviGene-1_0-ST Array (Affymetrix), which contained probe sets of over 22 047 known transcripts and expressed sequence tags. Gene Chips were washed and stained in the Affymetrix Fluidics Station 450. All arrays were scanned by Affymetrix® GeneChip Command Console (AGCC), which was installed in the GeneChip® Scanner 3000 7G. The RNA quality testing and quality control chart of microarray are provided in **Supplementary Figures 1, 2**. A normalized chip diagram is shown in **Supplementary Figure 3**.

Microarray Expression Data Analysis

Identification of Different Expression Genes (DEGs)

The data were analyzed with the Robust Multichip Analysis (RMA) algorithm using Affymetrix default analysis settings and global scaling as a normalization method. Values presented are log2 RMA signal intensity. The fold-change (FC) was calculated with fibrous ankylosis as control. DEGs were identified based on the t tests for comparison of the fibrous and bony ankylosis with a FC >2 and a P value <0.05. We used a volcano plot and heatmap to show the distribution of DEGs intuitively. The volcano plot and heatmap of the DEGs were drawn via ggplot2 and heatmap packages in R software [19].

Function Enrichment Analysis

The Gene Ontology (GO) term enrichment (http://www.geneontology.org/) was utilized to group the identified DEGs into defined categories of cellular component (CC), molecular function (MF), and biological process (BP) and determine which genes were significant [20]. Kyoto Encyclopedia of Genes and Genomes (KEGG) PATHWAY (http://www.genome.jp/kegg/pathway.html) was selected as the reference database for manually drawn pathway mapping [21]. The Database for Annotation, Visualization and Integration Discovery (DAVID, version 6.8, http://david. abcc.Ncifcrf.gov/) [22] was used to perform the GO and KEGG pathway enrichment analysis and ascertained the functions and pathways that might be disturbed by the identified DEGs, with the selected criterion of a P value <0.05.

Protein–protein Interaction Network Construction and Module Analysis

To evaluate the interactive relationships among DEGs, the protein–protein interaction pairs were executed using the String (Search Tool for the Retrieval of Interacting Genes, version 11.0; https://string-db.org/) [20], which is an online database

to assess and integrate physical and functional protein–protein associations with species limited to "Ovis aries" and an interaction score confidence >0.4 [23].

In PPI network, "node" represents a gene or protein, and "line" represents an interaction between 2 nodes. The degree of each node (number of interactions with other proteins) is equal to the number of nodes that interacted with this node. The hub nodes in the PPI net were those that scored highly as the network topology property indicators. Hub genes referred to the relatively key genes in the network, and they were identified by calculating 3 relationship characteristics in the PPI topological structure PPI network, including the degree centrality, betweenness centrality, and closeness centrality methods. By using the CytoNCA [24], a plug-in of Cytoscape, we completed the calculation, evaluation, and visualization of the methods mentioned above.

Significant modules in the PPI network were identified by molecular complex detection (MCODE) [25], a plug-in of Cytoscape software that clusters a network based on topology to recognize closely connected regions. The MCODE algorithm sorts and identifies each identified module. The higher the score is, the stronger the genes' association in this module. The parameters of DEGs clustering and scoring were set as follows: degree cutoff=2, node score cutoff=0.2, K-Core=2 and max depth=100.

Reverse Transcription and Real-time Polymerase Chain Reaction (PCR)

Ten interesting DEGs were selected from the microarray results to further confirm the reliability of the array data. Total RNA was isolated using Trizol reagent (Invitrogen Life Technologies, Carlsbad, USA) according to the manufacturer's instructions. Reverse transcription was performed with a cDNA synthesis kit (Promega, USA) in a 20 μL reaction system containing 2 μg total RNA [15].

Primers for each target gene were designed using the software of Primer Premier Version 5.0 and synthesized by Sangon Biotech (Shanghai) Co., Ltd, which are listed in **Table 1**. Quantitative real-time PCR was performed with the FastStart Universal SYBR Green Master (Roche, ref. 04913850001) using LightCycler 480 II Instrument (Roche, Switzerland). The reaction system and PCR cycle parameters were the same as previously described [10]. The housekeeping glyceraldehyde-3-phosphate dehydrogenase (GAPDH) gene was used for normalization of target genes expression. Relative mRNA expressions of the target genes between the fibrous and bony ankylosed callus were calculated using the $2^{-\Delta\Delta ct}$ method as previously described [10].

Table 1. Real-time PCR primer sequence.

Gene	Gene bank number	Primer sequences (5'-3')	Product size
GAPDH	AF030943.1	GCAAGTTCCACGGCACAG GGTTCACGCCCATCACAA	249 bp
COMP	XM_027969380.1	ACGCGCAGATAGACCCTAAC AACCAGCGTAGTCGTCATCC	165 bp
HAPLN1	XM_004009071.4	TCTGGGATATGACCGTTGCG TGCTTTAGGGTCACGCTCAG	188 bp
IBSP	XM_004009717.4	GTGGGGACAGTTATCGAGCC GCCACGCAAAATCCCAGAAG	144 bp
PRG4	XM_027975961.1	ATGGGAAAATAGTGGCGGCT TTGGGTGGGTTCCTGTTTGT	119 bp
TRPV4	XM_027956636.1	TGGAGCCCATCAACGAACTC GGTAAGGGTATGGCGGAGTG	153 bp
SYK	XM_027964185.1	GGCCATCCATACACACTGCT AGGGGTGAGGAGATGCTAGG	169 bp
CD86	NM_001038016.1	GCTTTCTGGTGCTGCTTCCTTC AAAGCTTGTGCGGCCTA T	210 bp
PTPRC	XM_027976000.1	CGGAAGTGAGCCTGTCTGAG TTGCTCACTCTCCTTGCTCG	245 bp

Statistical Analysis

The values of the fibrous and bony ankylosed callus were compared at each time-point. The Wilcoxon signed-rank test (SPSS 17.0) was conducted to determine whether statistical significance existed at *P* value <0.05.

Results

DEGs Between Fibrous and Bony Ankylotic Samples

All the DEGs at days 14 and 28 are shown in **S**upplementary Files 1 and 2. A total of 90 DEGs (70 upregulated in bony ankylosis and 20 upregulated in fibrous ankylosis) at day 14, and 323 DEGs (175 upregulated in bony ankylosis and 148 upregulated in fibrous ankylosis) at day 28 were found and illustrated by the volcano plots (**Figure 2A, 2B**). Five DEGs that co-expressed at days 14 and 28 were PRG4, GRIA1, LYVE1, ID1, and SLC7A2 (**Figure 2C**).

The represented DEGs at days 14 and 28 are shown in **Table 2**. The top 5 upregulated genes in bony ankylosis were LOC101119889 (FC=16.07), IGJ (FC=7.24), IGKV2-24 (FC=5.87), VNN2 (FC=5.54), and IGLV1-51 (FC=5.43) at day 14, and IBSP

(FC=268.53), COL10A1 (FC=70.25), SCRG1 (FC=52.96), PANX3 (FC=45.14), and OMD (FC=42.87) at day 28. The top 5 upregulated genes in fibrous ankylosis were PRG4 (FC=0.07), IL36B (FC=0.22), NNAT (FC=0.33), IL36A (FC=0.34), and ID1 (FC=0.38) at day 14, and PRG4 (FC=0.05), MMP1 (FC=0.08), MMP3 (FC=0.11), RGS4 (FC=0.16), and BRB (FC=0.18) at day 28.

The heat maps using hierarchical clustering analysis showed that the expression patterns of mRNAs between the 2 groups were significantly different both at day 14 (**Figure 2D**) and day 28 (**Figure 2E**) postoperatively, which indicated that the degree of severity of TMJ trauma can distinctively alter the gene expression patterns and eventually lead to different outcomes.

GO and KEGG Pathway Analyses of DEGs

The details of the GO and KEGG analysis results were presented in Supplementary Files 3 and 4.

At day 14, the 20 DEGs upregulated in fibrous ankylosis could be grouped into 3 BP terms through GO analysis (Supplementary File 3), which were relevant to negative regulation of osteoblast differentiation (GO: 0045668), hippocampus development (GO: 0021766), and positive regulation of interleukin-6 production (GO: 0032755).
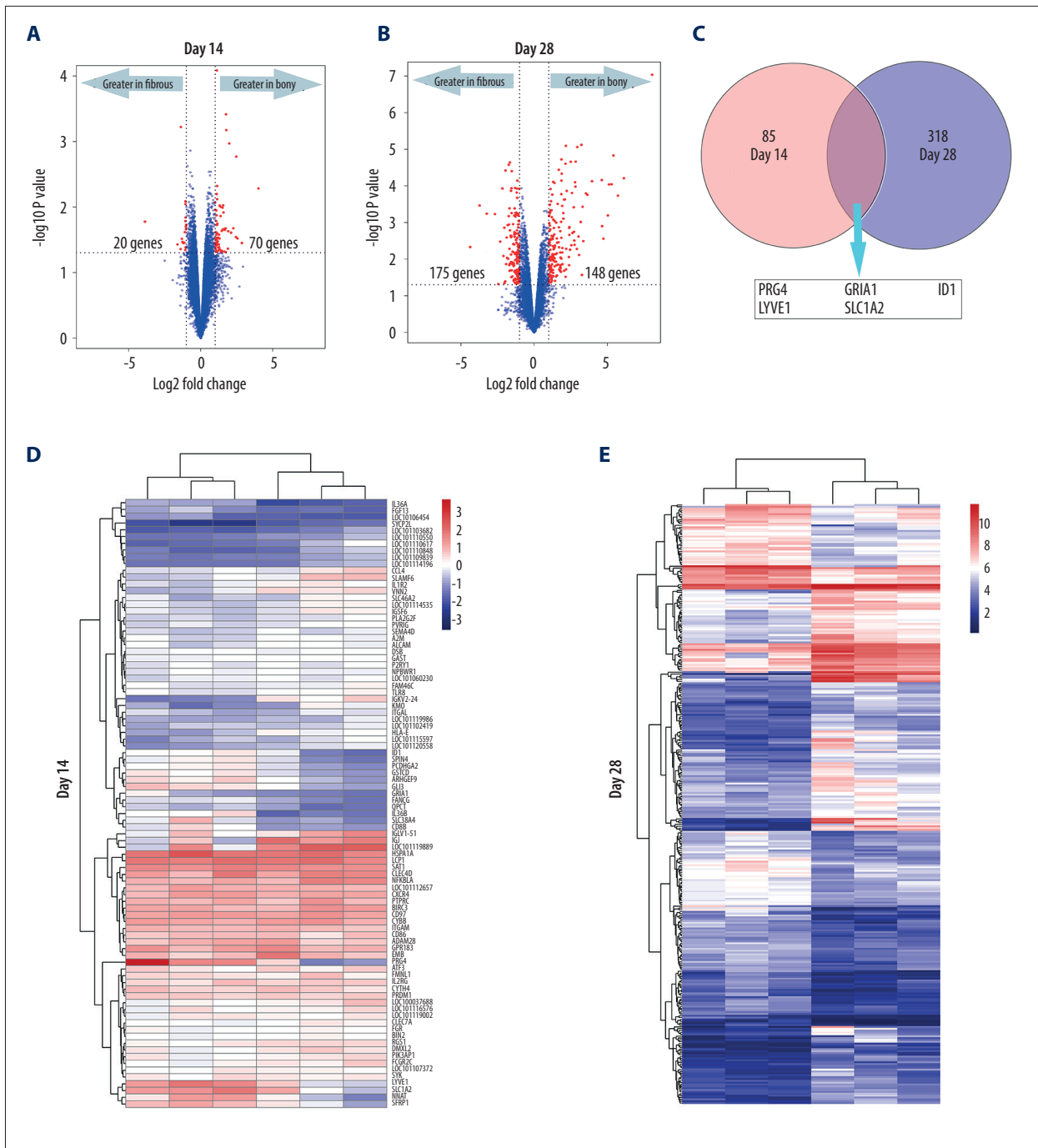
Figure 2. DEGs (fold-change >2, *P*<0.05) in the microarray profiles. (**A**) Volcano plot of 3 paired fibrous and bony ankylosed samples at day 14. (**B**) Volcano plot of 3 paired fibrous and bony ankylosed samples at day 28. (**C**) Venn diagram indicating that 5 mRNAs are co-expressed at both 2 time-points and their gene symbol are PRG4, GRIA1, LYVE1, ID1, SLC7A2. (**D**) Heat map of 3 paired fibrous and bony ankylosed samples at day 14. (**E**) Heat map of 3 paired fibrous and bony ankylosed samples at day 28. Different colors represent different expression levels (red high expression, white medium expression, and blue low expression). DEGs – differentially expressed genes.

Table 2. Representative differentially expressed genes (DEGs) between fibrous and bony ankylosis.

Upregulated in FA at day 14		Upregulated in BA at day 14		Upregulated in FA at day 28		Upregulated in BA at day 28	
Gene	Foldchange	Gene	Foldchange	Gene	Foldchange	Gene	Foldchange
PRG4	0.07	SYK	2.03	PRG4	0.05	BMP2	2.00
IL36B	0.22	FGR	2.05	MMP1	0.08	LRP4	2.00
NNAT	0.33	ITGAL	2.05	MMP3	0.11	CTGF	2.05
IL36A	0.34	ITGAM	2.07	RGS4	0.16	BMP4	2.18
ID1	0.38	CD86	2.10	BRB	0.18	IMPAD1	2.23
LYVE1	0.38	P2RY1	2.12	GPR1	0.20	FMOD	2.37
SLC38A4	0.40	FMNL1	2.15	PTHLH	0.22	TGFB2	2.38
SPIN4	0.42	ALCAM	2.20	STAC	0.22	TCF7	2.46
SLC7A2	0.43	SEMA4D	2.20	KYNU	0.23	SATB2	2.52
SFRP1	0.45	PRDM1	2.21	CDON	0.24	RUNX2	2.57
FANCG	0.46	CLEC7A	2.24	CCL21	0.24	SOX9	2.68
GRIA1	0.48	HSPA1A	2.26	STMN2	0.25	HHIP	2.93
PCDHGA2	0.48	CXCR4	2.35	OSR1	0.25	THBS4	2.98
CD8B	0.48	ATF3	2.36	RNASE6	0.26	CYR61	3.06
GSTCD	0.48	IL2RG	2.41	SERTM1	0.27	ITGA10	3.98
QPCT	0.48	PTPRC	2.42	FAM129A	0.27	ID1	4.15
ARHGEF9	0.48	TLR8	2.48	TMOD2	0.28	FGFR2	4.42
FGF13	0.49	CYBB	2.59	CCL23	0.29	FGFR3	5.18
GLI3	0.49	PIK3AP1	2.75	P2RY13	0.30	SP7	5.67
ZNF304	0.49	CLEC4D	3.13	NTN4	0.30	S100B	5.82
		IGSF6	3.19	GRIA1	0.30	TRPV4	6.70
		CCL4	3.34	LYVE1	0.31	SMOC2	7.08
		IL1R2	3.43	IL18	0.32	PTCH1	7.15
		NFKBIA	3.68	FGF10	0.34	ACAN	8.18
		KMO	3.75	TGFBR3	0.34	SERPINA1	8.41
		SLAMF6	4.80	TIAM1	0.34	MIA	9.08
		IGLV1-51	5.43	CD74	0.38	PTH1R	9.38
		VNN2	5.54	CXCL12	0.41	FRZB	9.62
		IGKV2-24	5.87	SLC7A2	0.41	PHOSPHO1	9.92
		JCHAIN	7.24	ITGB8	0.43	COL9A1	10.29
		LOC101119889	16.07	VEGFC	0.44	COL11A1	11.66
				VWF	0.44	SLC13A5	12.47
				CD44	0.44	LOC101119731	15.51

Table 2 continued. Representative differentially expressed genes (DEGs) between fibrous and bony ankylosis.

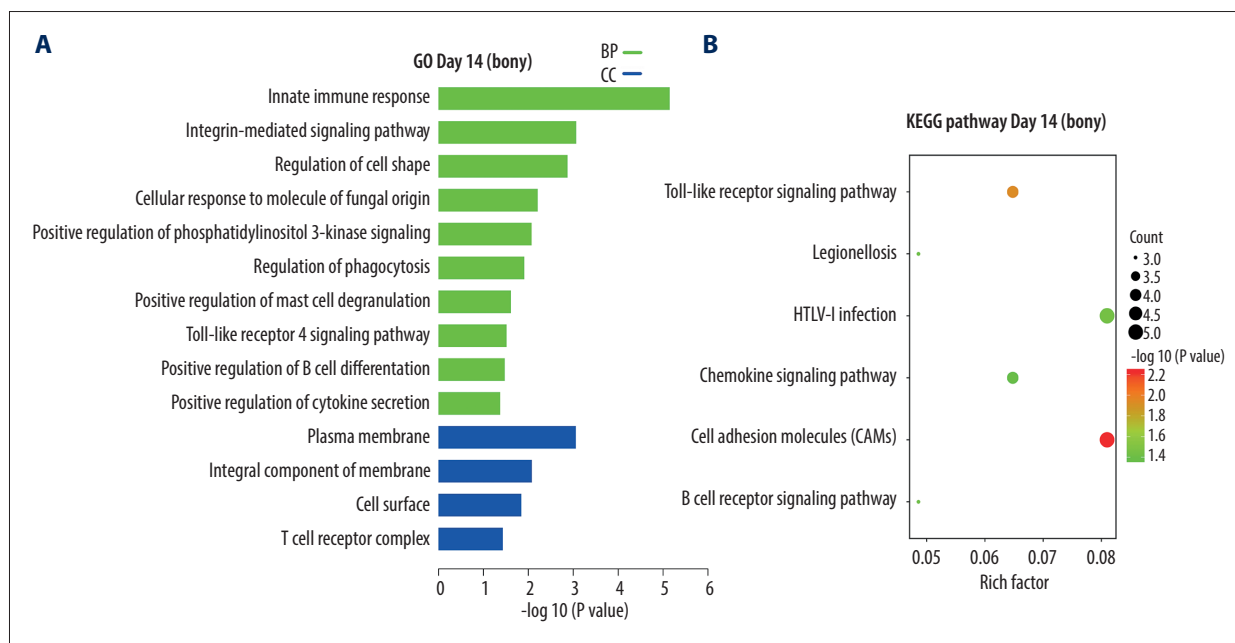| Upregulated in FA at day 14		Upregulated in BA at day 14		Upregulated in FA at day 28		Upregulated in BA at day 28	
Gene	Foldchange	Gene	Foldchange	Gene	Foldchange	Gene	Foldchange
				FLT4	0.45	CHAD	24.65
				COL5A3	0.45	COMP	25.07
				CSF1R	0.46	APOD	26.65
				KDR	0.46	ALPL	28.79
				DQA	0.47	CLEC3A	32.86
				NRP1	0.48	HAPLN1	34.75
				CDH5	0.49	COL2A1	39.18
						OMD	42.87
						PANX3	45.14
						SCRG1	52.96
						COL10A1	70.25
						IBSP	268.53

FA – fibrous ankylosis; BA – bony ankylosis.

Figure 3. KEGG and GO enrichment analysis for day14. (**A**) GO analysis of DEGs upregulated in bony ankylosis. The abscissa represents the -log10 (*P* value) of enrichment term, and the ordinate represents the enrichment term's names. (**B**) The KEGG pathway analysis of DEGs upregulated in bony ankylosis. The size of the circle represents gene count. The x-axis represents rich factor, and the y-axis represents pathway. Different circle colors represent different adjusted P values. GO – gene ontology; BP – biological process; CC – cellular component; MF – molecular function; KEGG – Kyoto Encyclopedia of Genes and Genomes; DEGs – differentially expressed genes.
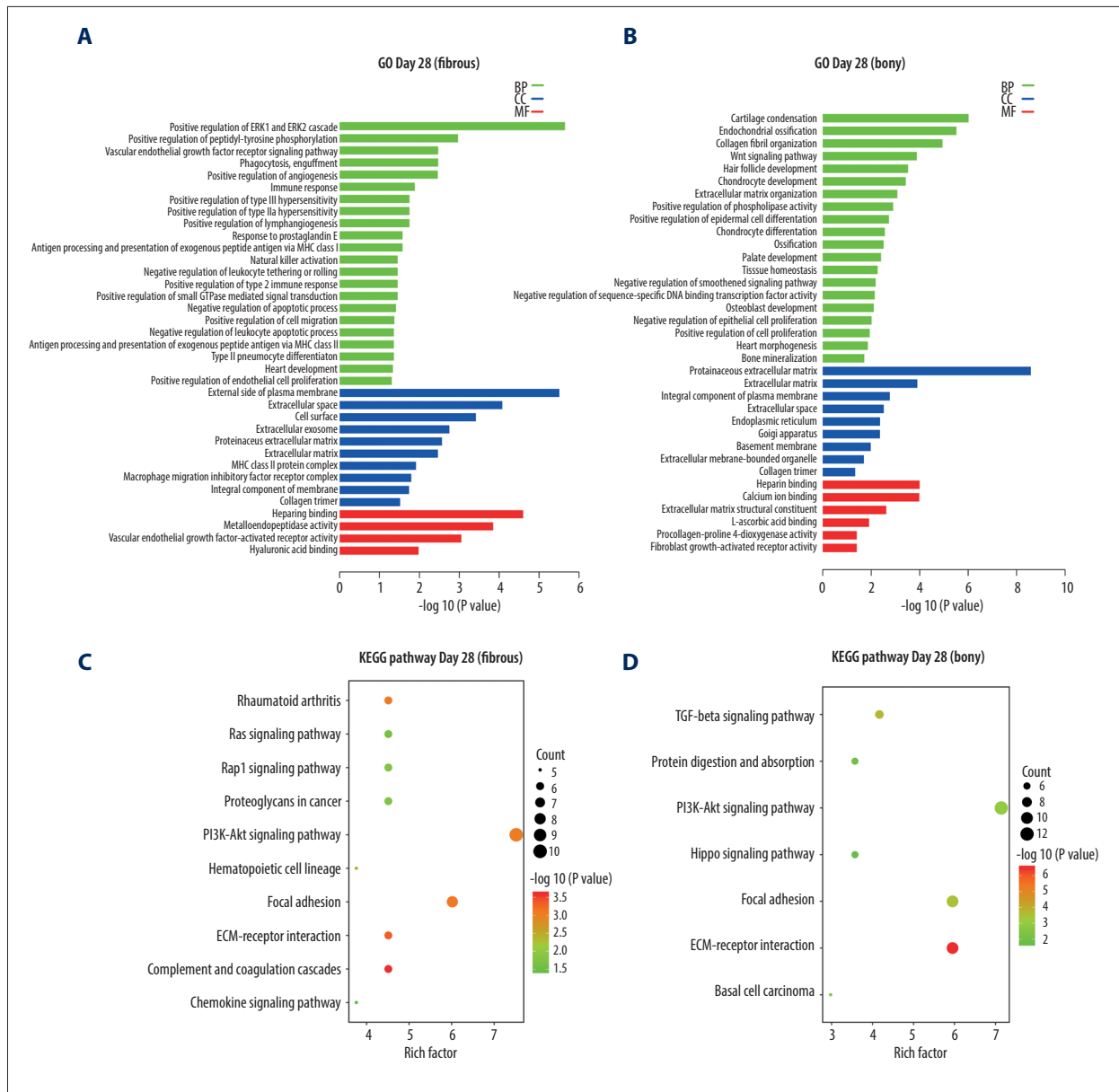
Figure 4. KEGG and GO enrichment analysis for day 28. (**A, B**) Representative GO analysis of DEGs upregulated in fibrous and bony ankylosis respectively. The abscissa represents the -log10 (*P* value) of enrichment term, and the ordinate represents the enrichment term's names. (**C, D**) Representative KEGG pathway analysis of DEGs upregulated in fibrous and bony ankylosis respectively. The size of the circle represents gene count. The x-axis represents rich factor, and the y-axis represents pathway. Different circle colors represent different adjusted P values. GO – gene ontology; BP – biological process; CC – cellular component; MF – molecular function; KEGG – Kyoto Encyclopedia of Genes and Genomes; DEGs – differentially expressed genes.

At day 14, the 70 DEGs upregulated in bony ankylosis could be enriched into 14 terms, including 10 in BP and 4 in CC (Supplementary File 3), and listed by the histogram according to the enrichment scores (**Figure 3A**). The BP terms were most relevant to innate immune response (GO: 0045087), integrin-mediated signaling pathway (GO: 0007229), regulation of cell shape (GO: 0008360), positive regulation of phosphatidylinositol 3-kinase signaling (GO: 0014068), Toll-like receptor 4 signaling pathway (GO: 0034142), and positive regulation of cytokine secretion (GO: 0050715). The CC terms were mostly associated with plasma membrane (GO: 0005886) and integral component of membrane (GO: 0016021). KEGG analysis of the 70 DEGs identified 6 enriched pathways, which are shown in a bubble diagram (**Figure 3B**). The representative pathways included cell adhesion molecules, Toll-like receptor signaling pathway, B cell receptor signaling pathway, and chemokine signaling pathway.

At day 28, the 148 DEGs upregulated in fibrous ankylosis could be grouped into 36 terms, including 22 in BP, 10 in CC, and 4 in MF, through GO analysis (Supplementary File 4), and are listed in the histogram (**Figure 4A**). The BP terms were most relevant to ERK1 and ERK2 cascade (GO: 0070374), peptidyl-tyrosine phosphorylation (GO: 0050731), immune response (GO: 0006955, GO: 0042590 and GO: 0030101), inflammation (GO: 0034695), angiogenesis (GO: 0045766, GO: 0001938 and GO: 0048010), and lymphangiogenesis (GO: 1901492). The CC terms were mostly enriched in plasma membrane (GO: 0009897 and GO: 0016021) extracellular (GO: 0005615, GO: 0070062, GO: 0005578 and GO: 0031012), cellular surface (GO: 0009986), and collagen trimer (GO: 0005581). The MF terms were closely related to heparin binding (GO: 0008201), metalloendopeptidase activity (GO: 0004222), VEGF-activated receptor activity (GO: 0005021), and hyaluronic acid binding (GO: 0005540). KEGG analysis of the 148 DEGs identified 15 pathways (Supplementary File 4), and the representative 10 pathways are shown in a bubble diagram (**Figure 4C**). Several pathways were interesting, for example, Complement and co-agulation cascades, ECM-receptor interaction, Focal adhesion, Rheumatoid arthritis, PI3K-AKt signaling, Rap1 signaling pathway, Ras signaling pathway, and Chemokine signaling pathway.

At day 28, the 175 DEGs upregulated in bony ankylosis could be grouped into 55 terms, including 40 in BP, 9 in CC, and 6 in MF through GO analysis (Supplementary File 4), and the representative 35 terms are listed in the histogram (**Figure 4B**). The BP terms were most relevant to cartilage condensation (GO: 0001502), chondrocyte development (GO: 0002063), chondrocyte differentiation (GO: 0002062), osteoblast development (GO: 0002076), endochondral ossification (GO: 0001958, GO: 0001503 and GO: 0030282), collagen fibril organization (GO: 0030199), Wnt signaling pathway (GO: 0016055), extracellular matrix organization (GO: 0030198), and phospholipase

activity (GO: 0010518). The CC terms mostly enriched in extracellular (GO: 0031012 and GO: 0005615), plasma membrane (GO: 0005887), endoplasmic reticulum (GO: 0005783), and Golgi apparatus (GO: 0005794). The MF terms were closely related to extracellular matrix structural constituent (GO: 0005201) and molecular binding, such as heparin binding (GO: 0008201), calcium ion binding (GO: 0005509), and L-ascorbic acid binding (GO: 0031418). KEGG analysis identified 9 pathways (Supplementary File 4), and the representative 7 pathways are shown in a bubble diagram (**Figure 4D**). Several pathways were interesting, for example, ECM-receptor interaction, TGF-beta signaling pathway, Focal adhesion, PI3K-Akt signaling pathway, and Protein digestion and absorption.

PPI Network Analysis

At day 14, the PPI network contained 44 nodes and 64 edges (**Figure 5A**). The top 10 hub genes with 24 edges were identified by CytoNCA (**Figure 5B**). In addition, only 1 significant module (MCODE score=5.4) consisting of 6 nodes and 14 edges in the PPI network was screened out by MCODE plug-in, which was composed of PTPRC, CD86, ITGAM, ITGAL, CXCR4, and SYK (**Figure 5C**).

A total of 222 nodes and 511 edges were identified from the DEGs at day 28 (**Figure 6A**). The top 10 hub genes with 28 edges were identified by CytoNCA (**Figure 6B**). By using MCODE analysis, 10 significant modules were screened out in the PPI network, and the most rewarding module (MCODE score=8.889) consisted of 10 nodes and 40 edges (**Figure 6C**).

Verification of differentially expressed mRNAs by real-time PCR

Ten interesting DEGs were selected for confirmation by quantitative real-time PCR analysis. Of these 10 DEGs, 7 were hub genes (SYK, CD86, ITGAM, ITGAL, PTPRC, IBSP, and COMP) according to PPI analysis. PRG4 was the top 1 gene upregulated at day 14 and the co-expressed gene upregulated at the 2 time-points. HAPLN1 was associated with bone formation and ankylosing spondylitis. TRPV4 was related to the mechanical environment and bone metabolism. We found that the expression pattern of the 10 genes (**Figure 7**) was similar to the microarray results, demonstrating a good correlation between the 2 methods.

At day 14, SYK (3.4-fold, P=0.029), CD 86 (2.2-fold, P=0.036), ITGAM (2.7-fold, P=0.033), ITGAL (3.6-fold, P=0.023) and PTPRC (3.7-fold, P=0.021) were upregulated, while PRG4 (55.7-fold, P=0.033) was downregulated in bony ankylosed callus in comparison to fibrous ankylosed callus (**Figure 7**). According to the GO and KEGG analyses, among the 5 hub genes, ITGAL, ITGAM, and SYK were relevant with integrin-mediated signaling
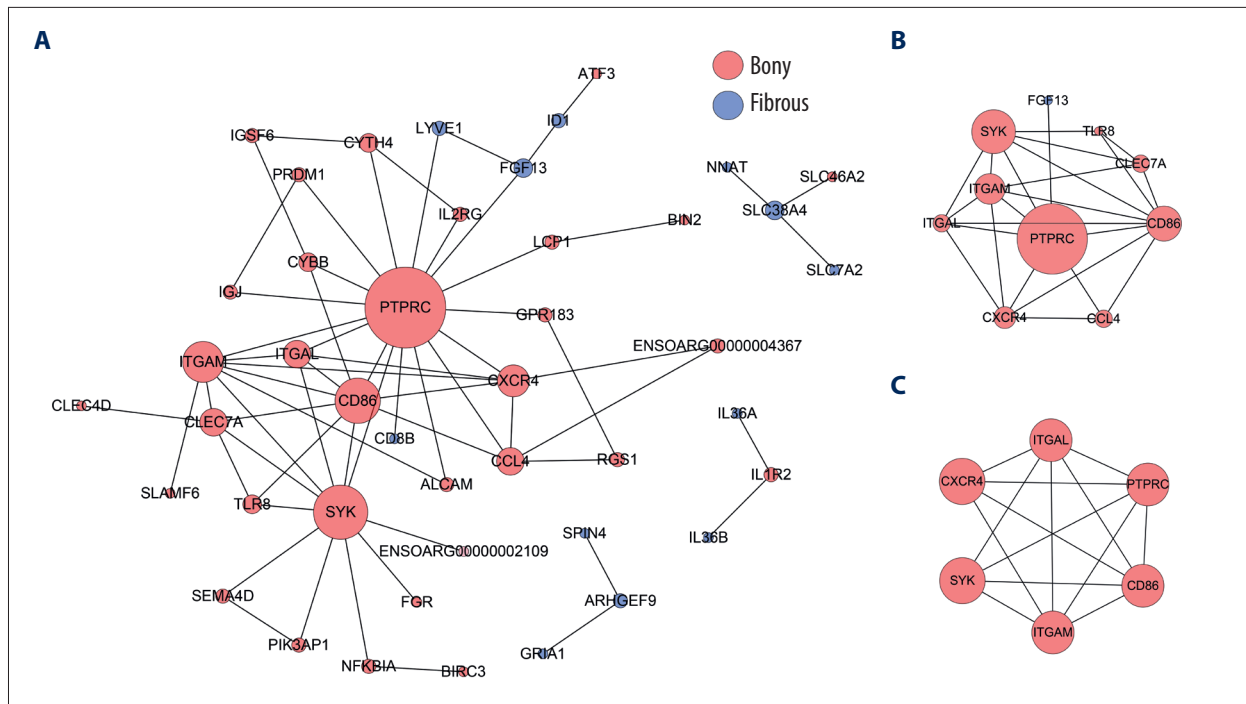
Figure 5. PPI network construction and Module analysis of the DEGs at day 14. (**A**) The PPI network of the DEGs consisted of 44 nodes and 64 edges. (**B**) The top 10 highly connected genes with 24 edges of PPI network. (**C**) The most significant module consisted of 6 nodes and 14 edges extracted from PPI network (MCODE score=5.4). The nodes represent proteins, and the edges between nodes represent interactions. The greater the degree of correlation, the larger the diameter of nodes. The nodes are red for upregulated in TMJ bony ankylosis, and blue for upregulation in fibrous ankylosis. PPI – protein–protein interaction; DEGs – differentially expressed genes.

pathway, and ITGAL, PTPRC, CD86, ITGAM were relevant with cell adhesion molecules (CAMs). Our results verified the 2 PPI pathways, indicating the enhanced integrin-mediated signaling pathway and cell adhesion during the development of bony ankylosis.

At day 28, bony ankylosis showed a significantly higher expression of COMP (2.7-fold, P=0.034), HAPLN1 (21.1-fold, P=0.021), IBSP (40.7-fold, P=0.008), and TRPV4 (3.1-fold, P=0.021), compared to fibrous ankylosis (**Figure 7**). However, the expression of PRG4 (50-fold, P=0.034) in fibrous ankylosis was significantly higher than that in bony ankylosis (**Figure 7B**).

Discussion

To the best of our knowledge, this is the first study to explore the different molecular mechanisms between fibrous and bony TMJ ankylosis by using transcriptome microarray profiles. In the present study, a total of 90 and 323 DEGs between TMJ fibrous and bony ankylosis were screened at days 14 and 28, respectively. According to GO annotations, these genes spanned many members of distinct functional families, encompassed many biological processes, and involved

many cellular components. Hierarchical clustering showed DEGs at day 28 had a clearer clustering than that at day 14 (**Figure 2D, 2E**), indicating that the genetic changes at day 14 were smaller than those at day 28; in other words, the major differences in the gene expression occurred at day 28. This result was not a surprise, because day 14 represented a relatively early stage of ankylosis, and the relatively small changes in the expression of mRNA corresponded to the actual beginning of different healing pathways, which was similar to the early process of fracture healing [26].

After integrating information from GO classifications and KEGG analyses at day 14, there appeared to be a series of molecular events that contributed to the onset of bony ankylosis. We found that the upregulated DEGs in bony ankylosis, such as CYBB, PIK3AP1, FGR, CLEC4D, CLEC7A, TLR8, SYK, and NFKBIA, were mainly involved in innate immunity response, Toll-like receptor (TLRs) signaling pathway, B cell receptor signaling, T cell receptor complex, and phagocytosis, indicating a stronger immune and inflammatory response occurred in bony ankylosis than in fibrous ankylosis. The results were reasonable because inflammation response plays a critical role in bone healing. Some pro-inflammatory molecules after initial acute injury, such as TNF-α and IL6, are essential for normal bone
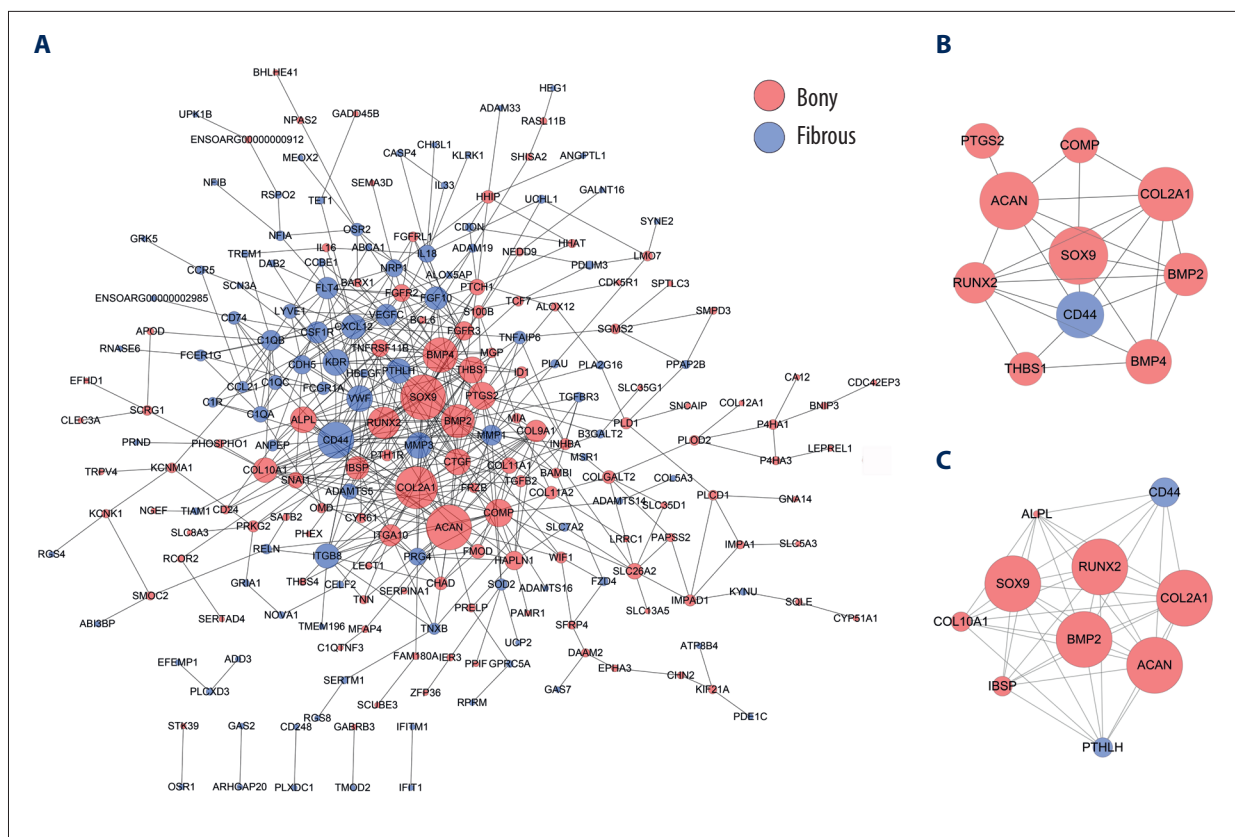
Figure 6. PPI network construction and Module analysis of the DEGs at day 28. (**A**) The PPI network of the DEGs consisted of 222 nodes and 511 edges. (**B**) The top 10 highly connected genes with 28 edges of PPI network. (**C**) The most significant module consisting of 10 nodes and 40 edges extracted from PPI network (MCODE score=8.889). The nodes represent proteins, and the edges between nodes represent interactions. The greater the degree of correlation, the larger the diameter of nodes. The nodes are red for upregulation in TMJ bony ankylosis, and blue for upregulation in fibrous ankylosis. PPI – protein–protein interaction; DEGs – differentially expressed genes.

formation during fracture healing [27], and a lack of them disturbs the bone healing and leads to nonunion [28,29]. The results also suggested that inhibiting the release of inflammatory cytokines in the early stage of bony ankylosis might be a promising approach to prevent its onset or delay its progression. In fact, a recently published study by Zhao et al [30] supports our findings. They found that large numbers of macrophages infiltrated in the early phase of ankylosis and that reducing macrophage numbers alleviated the progression of ankylosis by inhibiting cartilage formation [30].

The innate immune system is the first line of defense against microbes. Recently, the role of the innate immune system, and in particular TLRs, in the pathological changes of osteoarthritis, has been widely appreciated [31,32]. In the present study, our results indicated, for the first time, that the enhanced TLRs signaling pathway might be involved in the development of TMJ bony ankylosis. The results seemed reasonable since in the animal model the TMJ induced for bony ankylosis received more serious trauma than that for fibrous ankylosis. We inferred

that more dead cells, injured cells, and debris were produced due to more serious trauma, and they could release stronger endogenous cellular alarm signals to the antigen-presenting cells [33], thus resulting in stronger immune and inflammatory response. In this course, TLRs, as pattern recognition receptors, might play an important role in recognizing damage-related molecular pattern (DAMP), such as endogenous heat shock proteins, extracellular breakdown products of hyaluron, extracellular matrix (ECM) fragments, S100 proteins, high-mobility group box protein 1 (HMGB1), histones, and nucleic acids [33,34]. Signaling through cell surface TLRs could result in activation of the transcription factor NF-κB, with subsequent release of inflammatory cytokines, chemokines, and proteases [31,35], for example NFKBIA and interleukin, as shown in our results. These cytokines and chemokines can mediate neutrophil infiltration to the inflammatory site, and initiate an adaptive immune response [35,36]. Therefore, we thought that the activated TLR signaling pathway and the ensuing immune and inflammatory response might promote the onset of bony ankylosis, and deserved to be further studied.
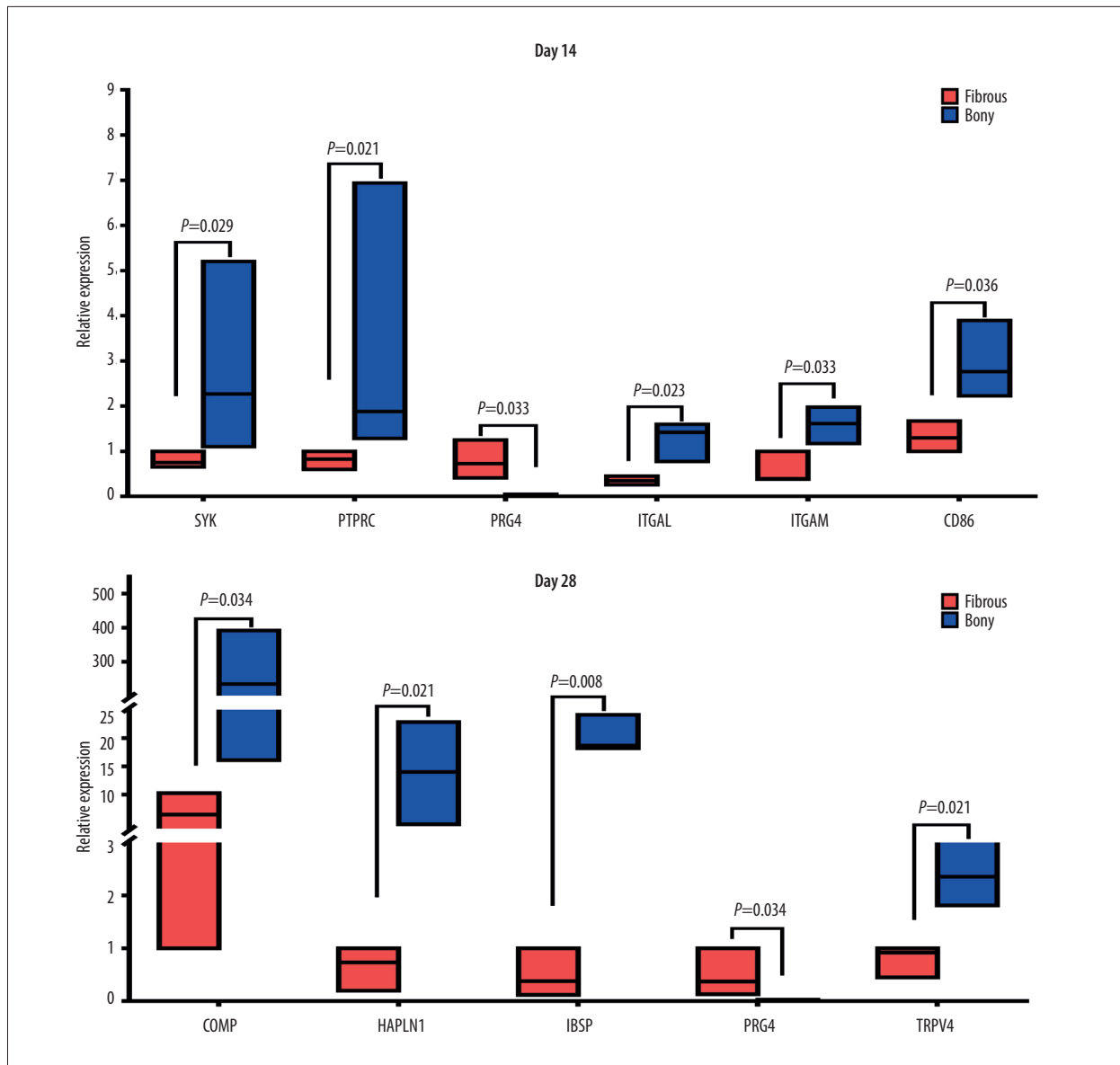
Figure 7. Real-time PCR analysis of the selected differentially expressed genes from the microarray results. Where given, the *P* values showed statistically significant differences between the fibrous and bony ankylosis at the indicated time-point.

At day 14, we found that bony ankylosis also showed upregulated integrin-mediated signaling pathway and cell adhesion molecules (CAMs), compared to fibrous ankylosis in the GO classifications and KEGG analyses. In addition, PPI analysis supported these results, since 5 of 6 hub genes, namely PTPRC (CD45), CD86, ITGAM (CD11b), SYK, and ITGAL (CD11a), were closely related with the integrin-mediated signaling pathway and CAMs. No direct correlation has been reported between cell adhesion and TMJ ankylosis up to now. However, during the wound healing, the cell-cell direct contact through CAMs is an important avenue for communication between resident cells in the injured tissue and the circulating effector cells [37]. As cell adhesion factors, ITGAL and ITGAM encode the alpha L

chain and the alpha M chain of integrins, respectively. αMβ2 (CD11b/CD18) and αLβ2 (CD11a/CD18), the 2 most broadly studied members of the β2 integrin subfamily, have diverse cell functions, including migration, adhesion, the respiratory burst, and cytokine production [38]. They play an important role in the trans-endothelial migration of leukocytes. After tissue damage, endothelial cell and white blood cell activation result in the extravasation of leukocytes into the wound site. The activated leukocyte and platelets release cytokines to upregulate the adhesion receptor on fibroblasts, macrophages, and epithelial cells, which in turn promotes their migration into the injured site [37]. We inferred that a similar situation may occur during the healing of TMJ trauma, and the increased

cell adhesion, especially mediated by ITGAL and ITGAM, might promote the formation of bony ankylosis. Further study is required to uncover their possible role in the pathogenesis of TMJ bony ankylosis.

Another 2 hub genes upregulated in bony ankylosis at day 14 were PTPRC and SYK. PTPRC was the hub gene with the highest degree at 14 days. Early-stage bone union is contingent upon the migration and proliferation of hematopoietic stem cells, endothelial progenitor cells, and mesenchymal stem cells [39]. PTPRC is a marker involved in proliferation, survival, and maintenance of hematopoietic stem cells and is expressed on the surface of all nucleated hematopoietic cells and their precursors, except mature erythrocytes and platelets [40]. A study showed that CD45+ hematopoietic cells from bone marrow were recruited into the site of fracture, and contributed to the inflammatory tissue formation [41]. SYK was the hub gene with the second highest degree at day 14. Belonging to the tyrosine kinase family, SYK is a critical component of signaling by a number of activating Fc-receptors on neutrophils, macrophages, and mast cells [42,43]. SYK is necessary for B cell receptor signaling and thus for B cell development [44,45]. In addition, SYK serves as an important tyrosine kinase in signal transduction following integrin engagement in hematopoietic cells [46]. The upregulated PTPRC and SYK in the bony ankylosis at day 14 seems to be involved in the immune and inflammatory response; however, their specific role needs further study.

Although in our animal model no cartilage formed in both types of ankylosed joint at day 14, a series of important differences in gene expressions at this time-point associated with ensuing histological differences. For example, genes involved in downregulation of the osteoblast differentiation pathway (SFRP1) [47] were upregulated in fibrous ankylosis. Interestingly, CXCR4 was upregulated in bone ankylosis and was a node in the most significant module in the PPI analysis. Studies have shown that CXCR4 can be responsible for the recruitment, migration, and homing of mesenchymal stem cells (MSCs) to the fracture site, and has chemotactic potential not only for inflammatory cells, but also for endothelial cells [39]. CXCR4 blockade negatively affected bone marrow cell migration toward the fracture site at least in the early phase of fracture healing [41]. Therefore, it seemed that the recruitment, migration, and differentiation of MSCs in different TMJ traumatic microenvironments might contribute to the onset of different types of ankylosis.

According to the GO analyses, bony ankylosis at day 28 showed increased BPs associated with new bone formation, such as cartilage condensation, endochondral ossification, chondrocyte development, chondrocyte differentiation, osteoblast development, bone mineralization, and ossification, which was in accordance with the histological presentation at the same

time. Accordingly, a series of key transcriptional factor regulating chondrocyte and osteoblast differentiation (Runx2, SOX9, SP7), center genes regulating endochondral ossification (BMP2, BMP4), and markers of chondrocyte and osteoblast (ALPL, COL2A1, COL10A1) were upregulated in bony ankylosis, which is consistent with our previous studies [15,16]. In addition, we also found that some new genes (eg, IBSP, COMP, HAPLN1, TRPV4, TGFB2, TCF7, FGFR2, FGFR3, SATB2, PTCH1, PTH1R), which have been previously demonstrated to be associated with bone formation [42,48-53], but not reported in TMJ ankylosis, were elevated in bony ankylosed joints. These new genes warrant further study to explore their possible roles in the development of bony ankylosis.

In contrast, fibrous ankylosis demonstrated increased BPs related with immune and inflammatory response at day 28, such as phagocytosis, immune response, response to prostaglandin E, natural killer cell activation, negative regulation of leukocyte apoptotic process, and antigen processing and presentation. Combined with the results of day 14, a prolonged immune and inflammatory reaction was a prominent feature of fibrous ankylosis. Normal bone healing is a well-orchestrated cascade of events, in which inflammatory and immune reaction initiates the regenerative healing process [54]. However, an unbalanced immune reaction will disturb the healing cascade and delays bone healing [55]. The inflammatory stage should resolve promptly, or the continued inflammatory response may inhibit bone formation [56]. Therefore, we thought that a prolonged inflammatory reaction contributed to the development of fibrous ankylosis.

Interestingly, 5 DEGs PRG4, LYVE1, GRIA1, SLC7A2, and ID1 were co-expressed at days 14 and 28 (**Figure 2C**). We found PRG4, LYVE1, GRIA1, and SLC7A2 were continuously upregulated in fibrous ankylosis from days 14 to 28, suggesting that these genes might play roles during the entire progression of fibrous ankylosis. Especially, PRG4 was the top 1 upregulated gene in fibrous ankylosis both at days 14 and 28. The PRG4 gene encodes lubricin, a mucin-like proteoglycan which is synthesized by superficial chondrocytes of the articular cartilage, synovial lining cells, and meniscal cells in synovial joints [57,58]. As the major component of synovial fluid, PRG4 covers the surface of normal articular cartilage and functions as a boundary lubricant to reduce friction and wear [59]. PRG4 exerts chondroprotective effects through preventing articular cartilage from friction-induced damage and inhibiting chondrocyte apoptosis [60,61]. PRG4 also has actions inhibiting cell adhesion and anti-inflammatory effects [58]. Recent studies revealed that the reduced level of PRG4 was associated with osteoarthritis since PRG4 was downregulated in an animal model of early osteoarthritis [62], and PRG4 null mice demonstrated rapid articular cartilage degeneration in TMJ as a lack of PRG4 [57,61]. In addition, parathyroid hormone (PTH), known for its anabolic actions in bone, can increases PRG4 expression to inhibit

articular cartilage degeneration, indicating PRG4 is a responsiveness gene mediating PTH chondroprotective properties [63,64]. In the present study, it seemed that PRG4 favored the development of fibrous ankylosis rather than bony ankylosis. PRG4 might exert anti-inflammatory and anti-adhesion effects to prevent the onset of bony ankylosis at day 14. Since fibrous ankylosis also showed upregulated PTHLH at day 28, we inferred that in the sheep model, PRG4 might act as the target gene of PTHLH to protect chondrocytes from death and inhibit cartilage degeneration, thereby alleviating the secondary damage to the articular surface, avoiding the further exposure of the bone marrow, and ultimately preventing the development of bony ankylosis. The present study indicated PRG4 is a promising target to inhibit the formation of bony ankylosis in the future; however, the specific mechanisms by which PRG4 exerts its inhibitory effects on bony ankylosis deserves to be further studied.

Sheep, rather than small animals such as mice and rats, were selected for animal modeling in this study because the structure and volume of the temporomandibular joint of sheep are similar to those of humans [13]. However, the corresponding methods of feeding, surgery, sampling, and subsequent analysis of the chip data are also complicated. The small number of animals used is an apparent limitation to the study design. In fact, only 3 sheep were used for each time-point in the present study. Because of the high risk of type II errors, the results of smaller studies are prone to greater sampling variation and hence are less precise. In addition, meaningful effects were probably missed due to the small sample. However, we used a self-control design, which can alleviate the individual differences, and the paired-sample t tests can also increase the sensitivity of statistical testing. Using a self-control design can also decrease the number of animals and complied with the principles of the replacement, refinement, or reduction (the 3Rs) for the use of animals in research. In a word, these results are preliminary and the strength of the current findings should not be overestimated given the small number of animals.

According to our previous animal studies, fibrous ankylosis was achieved on the condition that discectomy and condylar sagittal fracture were performed with minor damage to the glenoid fossa [10,11], while bony ankylosis occurred when severe damage to the glenoid fossa was performed combined with discectomy and condylar sagittal fracture [10,11]. The animal model was reliable and reproducible regardless of unilateral or bilateral TMJ surgery [10,11]. In the present study, the surgery process was consistent as reported in our previous studies, and the obvious histological differences between the 2 types of ankylosis at each time-point were also confirmed. Therefore, the molecular basis underlying the histological differences, as uncovered by microarray analysis of DEGs in the present study, was convincing, although the possibility that the whole-body circulation of cytokines/inflammation response might affect bilateral injury sites cannot be completely eliminated.

Conclusions

In conclusion, the present study shows a new and comprehensive expression profile of a large number of genes during the onset and progression of TMJ fibrous and bony ankylosis. New insights are provided for understanding of the molecular mechanisms underlying the association between the TMJ traumatic microenvironment and the types of ankylosis. Further investigation of the precise functional roles of these genes will provide new ideas for future treatment and prevention of TMJ bony ankylosis. Due to the preliminary and correlative nature of the datasets, further investigation and clinical justification of these genes should be done in the future, so as to provide new ideas for future treatment and prevention of TMJ bony ankylosis.

Ethics Statement

All protocols for animal experimentation were approved by the Ethics Committee of the Tianjin Stemmatological Hospital (Tianjin, China).

Conflict of Interests

None.

Supplementary Data

CNKINGBIO

The RNA quality testing (Day 14)

	Number	Sample	Concentration (ng/ul)	260/280	Volume (ul)	Total (ug)	Results
1	CT418092901	1_Fibro	668.4	2.04	20	13.37	A
2	CT418092902	2_Fibro	565.5	2.03	20	11.31	A
3	CT418092903	3_Fibro	267.3	1.96	20	5.35	A
4	CT418092904	1_bone	496.2	2.02	20	9.92	A
5	CT418092905	2_bone	544.2	2.04	20	10.89	A
6	CT418092906	3_bone	726.9	2.04	20	14.54	A

The RNA quality testing (Day 28)

|	Number	Sample	Concentration (ng/ul)	260/280	Volume (ul)	Total (ug)	Results
1	CT419071201	4_Fibro	454.0	2.06	40	18.2	A
2	CT419071202	5_Fibro	168.1	2.03	40	6.7	A
3	CT419071203	6_Fibro	334.6	2.03	40	13.4	A
4	CT419071204	4_bone	376.5	1.00	40	15.1	A
5	CT419071205	5_bone	316.3	1.93	40	12.7	A
6	CT419071206	6_bone	431.9	1.99	40	17.3	A

Supplementary Figure 1. The RNA quality control of each group of samples and the quality control results are all qualified.
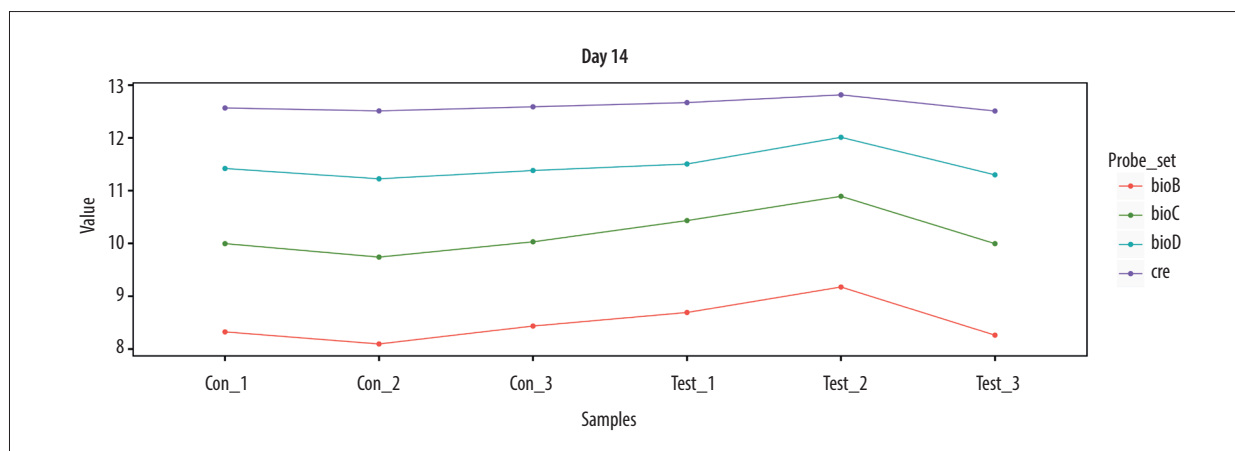
Supplementary Figure 2.1. (**Day 14**) Line chart of the chip quality control. The results of the microarray hybridization probe at 2 time-points were both bio B<bio C<bio D<Cre, indicating that the chip is qualified.
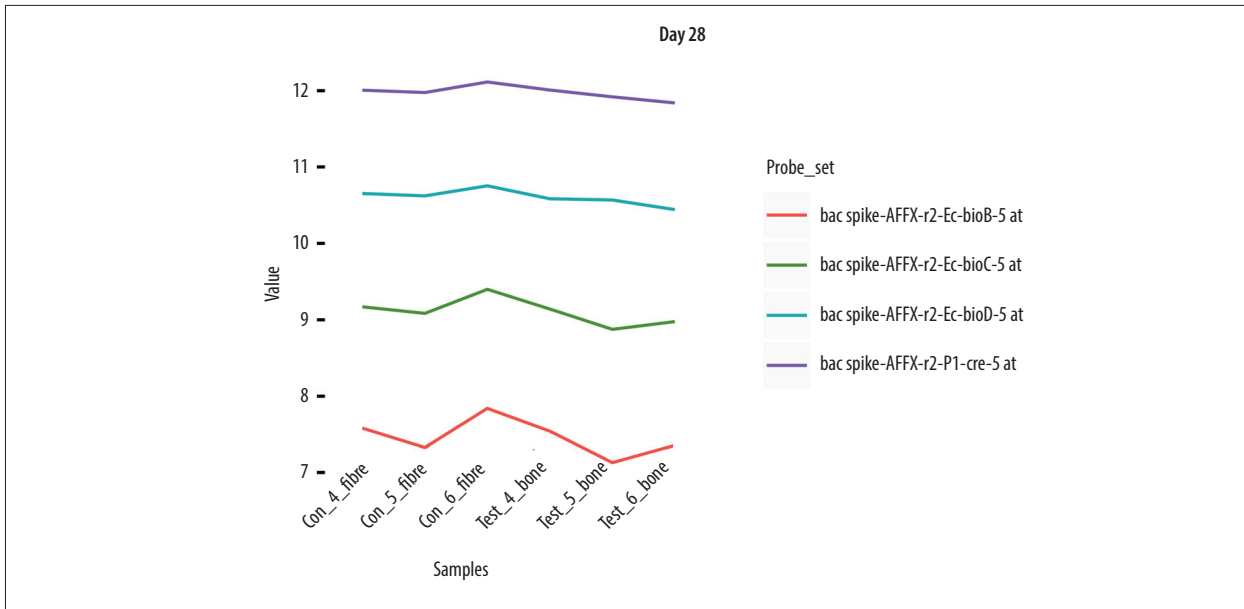
Supplementary Figure 2.2. (**Day 28**) Line chart of the chip quality control. The results of the microarray hybridization probe at 2 time-points were both bio B<bio C<bio D<Cre, indicating that the chip is qualified.
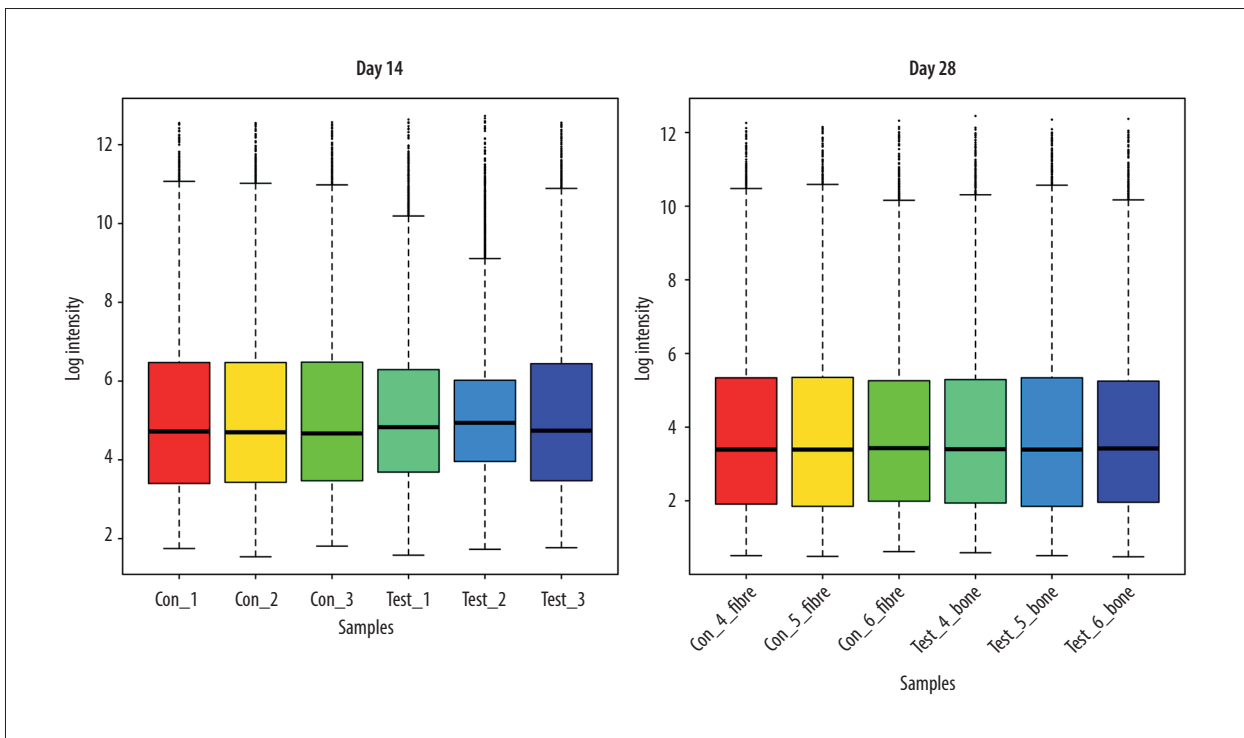
Supplementary Figure 3. Boxplot showing the expression distribution of each chip. All the chip's data have been normalized.

Supplementary Files 1-4.

Supplementary/raw Files available from the corresponding author on request.

References:

1. Jain G, Kumar S, Rana AS, et al. Temporomandibular joint ankylosis: A review of 44 cases. Oral Maxillofac Surg. 2008;12(2):61-66

2. Sawhney CP. Bony ankylosis of the temporomandibular joint: follow-up of 70 patients treated with arthroplasty and acrylic spacer interposition. Plast Reconstr Surg. 1986;77(1):29-40

3. Chidzonga MM. Temporomandibular joint ankylosis: Review of thirty-two cases. Br J Oral Maxillofac Surg. 1999;37(2):123-26

4. Erol B, Tanrikulu R, Gorgun B. A clinical study on ankylosis of the temporomandibular joint. J Craniomaxillofac Surg. 2006;34(2):100-6

5. Khanna JN, Ramaswami R. Protocol for the management of ankylosis of the temporomandibular joint. Br J Oral Maxillofac Surg. 2019;57(10):1113-18

6. Ko EC, Chen MY, Hsu M, Huang E, Lai S. Intraoral approach for arthroplasty for correction of TMJ ankylosis. Int J Oral Maxillofac Surg. 2009;38(12):1256-62

7. Li JM, An JG, Wang X, et al. Imaging and histologic features of traumatic temporomandibular joint ankylosis. Oral Surg Oral Med Oral Pathol Oral Radiol. 2014;118(3):330-37

8. He D, Ellis E 3rd, Zhang Y. Etiology of temporomandibular joint ankylosis secondary to condylar fractures: The role of concomitant mandibular fractures. J Oral Maxillofac Surg. 2008;66(1):77-84

9. Kaban LB, Bouchard C, Troulis MJ. A protocol for management of temporomandibular joint ankylosis in children. J Oral Maxillofac Surg. 2009;67(9):1966-78

10. Liang SX, Wang HL, Zhang PP, et al. Differential regulation of blood vessel formation between traumatic temporomandibular joint fibrous ankylosis and bony ankylosis in a sheep model. J Craniomaxillofac Surg. 2019;47(11):1739-51

11. Yan YB, Zhang Y, Gan YH, et al. Surgical induction of TMJ bony ankylosis in growing sheep and the role of injury severity of the glenoid fossa on the development of bony ankylosis. J Craniomaxillofac Surg. 2013;41(6):476-86

12. Yan YB, Liang SX, Shen J, et al. Current concepts in the pathogenesis of traumatic temporomandibular joint ankylosis. Head Face Med. 2014;10:35

13. Wang HL, Liu H, Shen J, et al. Removal of the articular fibrous layers with discectomy leads to temporomandibular joint ankylosis. Oral Surg Oral Med Oral Pathol Oral Radiol. 2019;127(5):372-80

14. Wang HL, Zhang PP, Meng L, et al. Preserving the fibrous layer of the mandibular condyle reduces the risk of ankylosis in a sheep model of intracapsular condylar fracture. J Oral Maxillofac Surg. 2018;76(9):1951.e1-24

15. Yan YB, Li JM, Xiao E, et al. A pilot trial on the molecular pathophysiology of traumatic temporomandibular joint bony ankylosis in a sheep model. Part I: Expression of Wnt signaling. J Craniomaxillofac Surg. 2014;42(2):e15-22

16. Yan YB, Li JM, Xiao E, et al. A pilot trial on the molecular pathophysiology of traumatic temporomandibular joint bony ankylosis in a sheep model. Part II: The differential gene expression among fibrous ankylosis, bony ankylosis and condylar fracture. J Craniomaxillofac Surg. 2014;42(2):e23-28

17. Meng J, Ma X, Ma D, Xu C. Microarray analysis of differential gene expression in temporomandibular joint condylar cartilage after experimentally induced osteoarthritis. Osteoarthritis Cartilage. 2005;13(12):1115-25

18. Zhang J, Sun X, Jia S, et al. The role of lateral pterygoid muscle in the traumatic temporomandibular joint ankylosis: A gene chip based analysis. Mol Med Rep. 2019;19(5):4297-305

19. Yi G, Liang M, Li M, et al. A large lung gene expression study identifying IL1B as a novel player in airway inflammation in COPD airway epithelial cells. Inflamm Res. 2018;67(6):539-51

20. Harris MA, Clark J, Ireland A, et al. The Gene Ontology (GO) database and informatics resource. Nucleic Acids Res. 2004;32(Database issue):D258-61

21. Kanehisa M, Goto S. KEGG: Kyoto encyclopedia of genes and genomes. Nucleic Acids Res. 2000;28(1):27-30

22. Huang DW, Sherman BT, Tan Q, et al. The DAVID Gene Functional Classification Tool: A novel biological module-centric algorithm to functionally analyze large gene lists. Genome Biol. 2007;8(9):R183

23. Szklarczyk D, Franceschini A, Wyder S, et al. STRING v10: Protein–protein interaction networks, integrated over the tree of life. Nucleic Acids Res. 2015;43(Database issue):D447-52

24. Tang Y, Li M, Wang J, Pan Y, Wu FX. CytoNCA: A cytoscape plugin for centrality analysis and evaluation of protein interaction networks. Biosystems. 2015;127:67-72

25. Bader GD, Hogue CW. An automated method for finding molecular complexes in large protein interaction networks. BMC Bioinformatics. 2003;4:2

26. Kolar P, Schmidt-Bleek K, Schell H, et al. The early fracture hematoma and its potential role in fracture healing. Tissue Eng Part B Rev. 2010;16(4):427-34

27. Gerstenfeld LC, Cullinane DM, Barnes GL, et al. Fracture healing as a postnatal developmental process: Molecular, spatial, and temporal aspects of its regulation. J Cell Biochem. 2003;88(5):873-84

28. Gerstenfeld LC, Cho TJ, Kon T, et al. Impaired fracture healing in the absence of TNF-alpha signaling: The role of TNF-alpha in endochondral cartilage resorption. J Bone Miner Res. 2003;18(9):1584-92

29. Yang X, Ricciardi BF, Hernandez-Soria A, et al. Callus mineralization and maturation are delayed during fracture healing in interleukin-6 knockout mice. Bone. 2007;41(6):928-36

30. Zhao L, Xiao E, He L, et al. Reducing macrophage numbers alleviates temporomandibular joint ankylosis. Cell Tissue Res. 2020;379(3):521-36

31. Miller RE, Scanzello CR, Malfait AM. An emerging role for Toll-like receptors at the neuroimmune interface in osteoarthritis. Semin Immunopathol. 2019;41(5):583-94

32. Jung YK, Park HR, Cho HJ, et al. Degrading products of chondroitin sulfate can induce hypertrophy-like changes and MMP-13/ADAMTS5 production in chondrocytes. Sci Rep. 2019;9(1):15846

33. Matzinger P. The danger model: A renewed sense of self. Science. 2002;296(5566):301-5

34. van den Bosch MHJ. Inflammation in osteoarthritis: Is it time to dampen the alarm(in) in this debilitating disease? Clin Exp Immunol. 2019;195(2):153-66

35. Bender AT, Tzvetkov E, Pereira A, et al. TLR7 and TLR8 differentially activate the IRF and NF-kappaB pathways in specific cell types to promote inflammation. Immunohorizons. 2020;4(2):93-107

36. Gay NJ, Symmons MF, Gangloff M, Bryant CE. Assembly and localization of Toll-like receptor signalling complexes. Nat Rev Immunol. 2014;14(8):546-58

37. Albelda SM, Buck CA. Integrins and other cell adhesion molecules. FASEB J. 1990;4(11):2868-80

38. Tan SM. The leucocyte β2 (CD18) integrins: The structure, functional regulation and signalling properties. Biosci Rep. 2012;32(3):241-69

39. Yellowley C. CXCL12/CXCR4 signaling and other recruitment and homing pathways in fracture repair. Bonekey Rep. 2013;2:300

40. Kiel MJ, Yilmaz OH, Iwashita T, et al. SLAM family receptors distinguish hematopoietic stem and progenitor cells and reveal endothelial niches for stem cells. Cell. 2005;121(7):1109-21

41. Asiedu KO, Ferdousi M, Ton PT, et al. Bone marrow cell homing to sites of acute tibial fracture: (89)Zr-oxine cell labeling with positron emission tomographic imaging in a mouse model. EJNMMI Res. 2018;8(1):109

42. Hu K, Sun H, Gui B, Sui C. TRPV4 functions in flow shear stress induced early osteogenic differentiation of human bone marrow mesenchymal stem cells. Biomed Pharmacother. 2017;91:841-48

43. Sedlik C, Orbach D, Veron P, et al. A critical role for Syk protein tyrosine kinase in Fc receptor-mediated antigen presentation and induction of dendritic cell maturation. J Immunol. 2003;170(2):846-52

44. Cheng AM, Rowley B, Pao W, et al. Syk tyrosine kinase required for mouse viability and B-cell development. Nature. 1995;378(6554):303-6

45. Turner M, Mee PJ, Costello PS, et al. Perinatal lethality and blocked B-cell development in mice lacking the tyrosine kinase Syk. Nature. 1995;378(6554):298-302

46. Jakus Z, Fodor S, Abram CL, et al. Immunoreceptor-like signaling by beta 2 and beta 3 integrins. Trends Cell Biol. 2007;17(10):493-501

47. Gaur T, Rich L, Lengner CJ, et al. Secreted frizzled related protein 1 regulates Wnt signaling for BMP2 induced chondrocyte differentiation. J Cell Physiol. 2006;208(1):87-96

48. Yu L, Xu Y, Qu H, et al. Decrease of MiR-31 induced by TNF-alpha inhibitor activates SATB2/RUNX2 pathway and promotes osteogenic differentiation in ethanol-induced osteonecrosis. J Cell Physiol. 2019;234(4):4314-26

49. Qin X, Jiang Q, Miyazaki T, Komori T. Runx2 regulates cranial suture closure by inducing hedgehog, Fgf, Wnt and Pthlh signaling pathway gene expressions in suture mesenchymal cells. Hum Mol Genet. 2019;28(6):896-911

50. Yu S, Li J, Zhao Y, Li X, Ge L. Comparative secretome analysis of mesenchymal stem cells from dental apical papilla and bone marrow during early odonto/osteogenic differentiation: Potential role of transforming growth factor-beta2. Front Physiol. 2020;11:41

51. Goodwin AF, Chen CP, Vo NT, et al. YAP/TAZ regulate elevation and bone formation of the mouse secondary palate. J Dent Res. 2020;99(12):1387-96

52. Jeong BC, Kim HJ, Bae IH, et al. COMP-Ang1, a chimeric form of Angiopoietin 1, enhances BMP2-induced osteoblast differentiation and bone formation. Bone. 2010;46(2):479-86

53. Dudhia J, Bayliss MT, Hardingham TE. Human link protein gene: Structure and transcription pattern in chondrocytes. Biochem J. 1994;303(Pt 1):329-33

54. Schmidt-Bleek K, Schell H, Schulz N, et al. Inflammatory phase of bone healing initiates the regenerative healing cascade. Cell Tissue Res. 2012;347(3):567-73

55. Mountziaris PM, Spicer PP, Kasper FK, Mikos AG. Harnessing and modulating inflammation in strategies for bone regeneration. Tissue Eng Part B Rev. 2011;17(6):393-402

56. Thomas MV, Puleo DA. Infection, inflammation, and bone regeneration: A paradoxical relationship. J Dent Res. 2011;90(9):1052-61

57. Hill A, Duran J, Purcell P. Lubricin protects the temporomandibular joint surfaces from degeneration. PLoS One. 2014;9(9):e106497

58. Edsfeldt S, Holm B, Mahlapuu M, et al. PXL01 in sodium hyaluronate results in increased PRG4 expression: A potential mechanism for anti-adhesion. Ups J Med Sci. 2017;122(1):28-34

59. Nakagawa Y, Muneta T, Otabe K, et al. Cartilage derived from bone marrow mesenchymal stem cells expresses lubricin in vitro and in vivo. PLoS One. 2016;11(2):e0148777

60. Wang Q, Tan QY, Xu W, et al. Cartilage-specific deletion of Alk5 gene results in a progressive osteoarthritis-like phenotype in mice. Osteoarthritis Cartilage. 2017;25(11):1868-79

61. Koyama E, Saunders C, Salhab I, et al. Lubricin is required for the structural integrity and post-natal maintenance of TMJ. J Dent Res. 2014;93(7):663-70

62. Young AA, McLennan S, Smith MM, et al. Proteoglycan 4 downregulation in a sheep meniscectomy model of early osteoarthritis. Arthritis Res Ther. 2006;8(2):R41

63. Novince CM, Entezami P, Wilson CG, et al. Impact of proteoglycan-4 and parathyroid hormone on articular cartilage. J Orthop Res. 2013;31(2):183-90

64. Novince CM, Michalski MN, Koh AJ, et al. Proteoglycan 4: A dynamic regulator of skeletogenesis and parathyroid hormone skeletal anabolism. J Bone Miner Res. 2012;27(1):11-25

e932545-19

Indexed in: [Current Contents/Clinical Medicine] [SCI Expanded] [ISI Alerting System]
[ISI Journals Master List] [Index Medicus/MEDLINE] [EMBASE/Excerpta Medica]
[Chemical Abstracts/CAS]